JOURNAL OF AIRCRAFT
Vol. 42, No. 3, May–June 2005

Study of Four-Vortex Aircraft Wakes and Layout of Corresponding Aircraft Configurations

Eike Stumpf*
DLR German Aerospace Center, 38108 Braunschweig, Germany

A sequence of numerical simulations for the efficient determination of four-vortex wakes, consisting of two counter-rotating vortex pairs, with low induced rolling moments after the unstable merging of inner and outer vortices, is proposed. After a systematic investigation of generic four-vortex systems in a second step, an airliner geometry in high-lift configuration is modified such that it produces a vortex wake similar to the identified optimal four-vortex system. The configuration modification is done using simple design rules. For verification of the existence of a similar four-vortex system, the wake vortex of the modified airliner configuration is simulated up to the extended near field in a final step. Two four-vortex configurations are considered in the present paper, different only in the vortex spacing ratio. A maximum reduction of rolling moment down to 44–52% of the rolling moment of a reference two-vortex system is achieved within a distance equivalent to 2.89 n miles for a real size Airbus A340. The realization of four-vortex wakes behind an individually modified high-lift configuration similar to the aforedetermined promising generic four-vortex configurations is demonstrated.

Nomenclature

b	=	span
c_L	=	total lift coefficient
c_R	=	rolling-moment coefficient
E_{kin}	=	two-dimensional kinetic energy
M	=	Mach number
p_{tot}	=	total pressure loss
r	=	radius
t	=	time
t^*	=	normalized time, $= [\Gamma_1/(2\pi b_1^2)]t$
u, v, w	=	velocity components
x, y, z	=	Cartesian body axes
α	=	angle of attack
Γ	=	circulation
δ	=	deflection angle
Λ	=	aspect ratio
λ	=	wavelength
σ	=	amplification rate
ω	=	vorticity

Subscripts

exp.	=	experiment
f	=	following aircraft
HTP	=	horizontal tail plane
iflap	=	inner flap
sim.	=	simulation
x	=	axial component
Θ	=	circumferential component
0	=	initial value
1	=	outer vortex pair
2	=	inner vortex pair
$2V$	=	two-vortex reference system
∞	=	freestream value

Presented as Paper 2004-1067 at the 42nd Aerospace Sciences Meeting and Exhibit, Reno, NV, 5–8 January 2004; received 22 January 2004; revision received 7 May 2004; accepted for publication 11 May 2004.

*Research Engineer, Institute of Aerodynamics and Flow Technology; eike.stumpf@dlr.de.

Introduction

WORLD airports face a long-term capacity problem as a result of the separation standards presently in use. These air traffic control separation regulations determine the minimum longitudinal distance between two aircraft on the same flight path dependent on the maximum takeoff weights of both aircraft in order to prevent the following aircraft from encountering potentially hazardous wake turbulence. For an alleviation of wake vortices, it seems most promising to make use of the inherent instabilities of vortex systems: either by triggering actively a specific wavelength with counteracting flaps and spoilers as proposed by Crow and Bate[1] and patented by the Boeing Corporation[2] or by designing a highly unstable vortex system for which natural perturbations from the aircraft boundary layer or weak atmospheric turbulence are sufficient for an onset of instability.

For the investigation of the latter approach, the complex topology of a high-lift configuration vortex wake is generally reduced to a four-vortex system, consisting of two pairs of counter-rotating vortices (see Fig. 1). These represent on either side of the symmetry plane respectively the merged vortices of the wing tip and outer-flap side edge and the merged vortices of the inner-flap side edge and horizontal tail. Following numerical simulations by Fabre and Jacquin[3] and Fabre et al.[4] the amplification rate of inherent instabilities on such vortex systems is one order of magnitude higher and the wavelength nearly one order of magnitude smaller compared to the Crow instability on a single counter-rotating vortex pair.

A four-vortex system (see Fig. 1) is defined by four parameters: the vortex spacing ratio b_2/b_1, with b_1 resp. b_2 being the spacing of the counter-rotating vortices of the two pairs, Γ_2/Γ_1 the ratio of their circulations and the normalized vortex core radii r_1/b_1 and r_2/b_1.

The specific interest on the temporal development of four-vortex systems arose because the knowledge might contribute to the understanding of University of California, Berkeley towing-tank, ONERA catapult and NASA free-flight tests by Ortega,[5] Coton,[6] Stuff,[7] and Rossow,[8] respectively, which were successful regarding wake-vortex hazard alleviation. In all three experiments basically a four-vortex wake developed, which led to a substantial rolling-moment reduction during the unstable merging process of the inner and outer vortices.

Based on these promising results in the present paper, a sequence of numerical simulations is proposed whose starting point is a systematic investigation of generic four-vortex systems in order to identify a four-vortex topology resulting in minimum rolling moments. In a second step the considered airliner geometry, here exemplary the DLR-F11 model in high-lift configuration (see Fig. 2), is modified

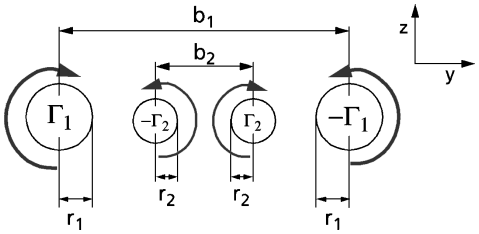

Fig. 1 Four-vortex system.

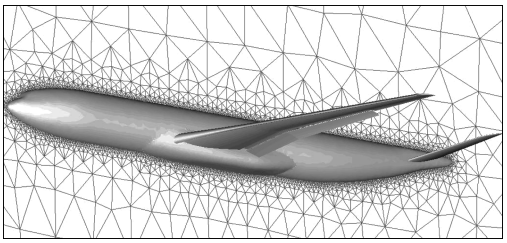

Fig. 2 DLR-F11 model.

by hand such that it produces a vortex wake resembling the identified optimal four-vortex system. The configuration modification is done using simple design rules as can be found in textbooks, for example, Torenbeek.[9] For a verification of the existence of a resembling four-vortex system, the wake vortex of the modified airliner configuration is simulated up to the extended nearfield in a final step.

The aim of the present paper is to show that this sequence of numerical simulations allows the modification of high-lift configurations resulting in less harmful vortex wakes. At this stage the sequence is not mature enough to be included in the regular design process, rather the presented results should be seen as a proof of concept.

Sequence of Numerical Simulations

For the proposed sequence of numerical simulations, two different flow solvers are employed: the large-eddy simulation/direct numerical simulation (LES/DNS) code National Center for Atmospheric Research, Boulder, Colorado (NCAR)-EuLag[10] and the Euler/Reynolds-averaged Navier–Stokes, code DLR-TAU.[11]

NCAR-EuLag

In the first and third step[5] of the sequence, NCAR-EuLag[10] is used. EuLag was developed at NCAR for meteorological and geophysical applications and is based on the nonoscillatory advection scheme MPDATA (multidimensional positive definite advection transport algorithm) by Smolarkiewicz.[12] EuLag is a pure advection scheme; no diffusive fluxes are explicitly considered. The advection is calculated in a first pass by a first-order-accurate upstream differencing predictor step. A second pass, as a corrector step, increases the accuracy of the calculation to second order by estimating and compensating the truncation error of the first pass. In the present paper EuLag is used for monotonically integrated large-eddy simulations (MILES), as originally proposed by Boris et al.[13] In MILES the incompressible Navier–Stokes equations are discretized on a coarse LES mesh without introducing neither a filtering operation nor a subgrid-scale stress tensor. The use of EuLag for MILES has been validated for decaying isotropic turbulence by Domradzki et al.[10] and vortical flows by Dörnbrack et al.[14]

DLR-TAU

In the third step of the sequence besides NCAR-EuLag, the DLR-TAU code[11] is employed. The DLR-TAU code is a finite volume Euler/Navier–Stokes solver working on unstructured and hybrid grids. Local time stepping and multigrid for convergence acceleration are included. The inviscid fluxes are calculated by employing a second-order central scheme with scalar dissipation. A grid-adaptation module enables the primary grid to be adapted to the solution if an enhanced resolution is required in certain regions of the computational domain. As an indicator for the adaptation, the total pressure gradient is used. In the present paper the DLR-TAU code is solely utilized for Euler computations.

Sequence of Flow Solvers

A standard approach for the simulation of vortex wakes would start with the simulation of the flowfield around the airplane geometry up to a short distance behind the rear end of the fuselage and continue with coupled computational domains in order to cover at least a part of the wake-vortex far field, as for example shown by the author.[15] However, this approach requires the simulation of the complete vortex wake for each considered configuration, that is, a huge amount of CPU-h, and is therefore unsuitable for systematic investigations.

In contrast the proposed sequence of numerical simulations represents an inverse approach, that is, the starting point is a generic four-vortex configuration as displayed left of the bold vertical line in Fig. 3. The total circulation and the vortex centroid position of this four-vortex configuration should roughly correspond to the considered aircraft geometry. For the temporal simulation, the first step in the sequence, the EuLag code is used for three-dimensional-MILES of the chosen four-vortex system. The vortices are initialized as straight vortex tubes with superimposed weak atmospheric turbulence [$v_{\mathrm{rms}}^{'} = 0.005 \max(v_\Theta)$]. Without exact knowledge of the corresponding aircraft geometry, the four-vortex system parameters can be successively varied in subsequent calculations in order to identify a four-vortex configuration with minimum induced rolling moment.

Once the parameters of a promising four-vortex configuration are determined, the considered aircraft configuration is modified as indicated in the central part of Fig. 3. For the modification simple design rules are used, as can be found in textbooks. The aim of the modification is to obtain a vortex-wake topology behind the modified aircraft configuration that resembles the identified promising four-vortex system.

For a verification of the success of the modification, a stepwise simulation of the vortex wake of the modified airliner configuration is carried out with the DLR-TAU and NCAR-EuLag code. The flow around the aircraft is computed in a steady three-dimensional Euler simulation with the flow solver DLR-TAU. The computational domain extends 40 spans in all directions, but the grid size limitation allows only a sufficient resolution of the vortex wake near field. Thus, a plane extracted at $x/b = 0.5$ immediately downstream of the rear end of the fuselage (point of origin is the trailing edge of the wing tip) serves to initialize a temporal two-dimensional simulation of the roll-up process. It has been shown for example by de Bruin et al.[16] that two-dimensional simulations are capable to simulate the roll-up process in good agreement to measurement results. Here, temporal two-dimensional EuLag simulations of the extended near field equivalent to a downstream distance of $x/b = 10$ are carried out. Within 10 spans the vorticity sheets and discrete vortices should

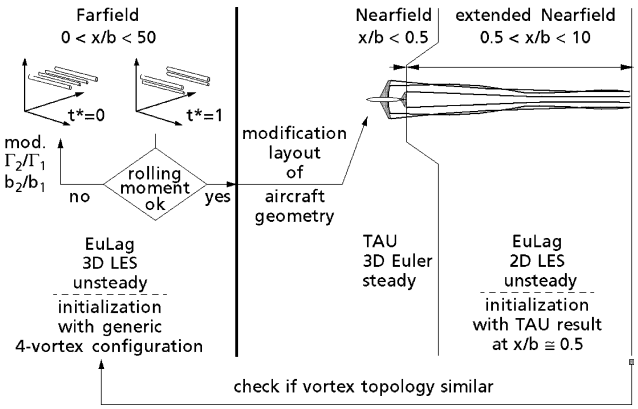

Fig. 3 Numerical strategy.

have merged into a simple four-vortex system. The quantitative analysis of the vortex topology in terms of circulation and spacing ratio at $x/b = 10$ reveals whether a vortex system similar to the optimal one is produced. If not, the layout has to be redone in an iterative process.

Validation

The components of the proposed sequence of numerical simulations are validated separately: the near- and extended near-field calculations are validated with wind-tunnel measurements described by Coustols et al.,[17] and the far-field simulation is validated with measurement results from Ortega[5] and linear instability calculations done by Fabre (personal communication, 2003).

Near- and Extended Near-Field Validation

For the validation of the near- and extended near-field calculations, wind-tunnel five-hole probe data are available in two downstream planes at $x/b = 0.5$ and 6 from the European research project C-Wake. Details of the measurements can be found in Coustols et al.[17] The aircraft model used is the DLR-F11 (see Fig. 2). That is a wide-body airliner model with a span $b = 2.8$ m, sharp-edged wing and flap tips and blunt trailing edges. Investigated is the standard takeoff configuration with flap deflection angles $\delta_{\text{Flap}} = 22$ deg and a slat deflection of $\delta_{\text{Slat}} = 20$ deg. The angle of attack in the experiment was $\alpha_{\text{exp.}} = 13.1$ deg, and the horizontal tail was set to $\delta_{\text{HTP,exp.}} = -15$ deg. Flow condition of the test was $M_\infty = 0.2$, ambient temperature, and pressure. Because Euler calculations overpredict lift considerably, the angle of attack and the deflection angle of the horizontal tail are adjusted for the calculation based on benchmark test results by the author and colleagues[18] in order to achieve the measured lift coefficient of $c_L = 1.76$. This leads to an α reduction of $\Delta\alpha_{\text{sim.}} = -1$ deg and a less deflected horizontal tail with $\delta_{\text{HTP,sim.}} = -14$ deg. The mesh for the near-field Euler calculation with DLR-TAU is generated with the commercial tool ICEM Tetra. The basic mesh contains 1.1×10^6 grid points, the seven times adapted mesh 4.8×10^6 grid points. A comparison of the experiment and the Euler calculation result on the seven times adapted mesh is shown in a plane a half-span downstream of the wing-tip trailing edge ($x/b = 0.5$) in Fig. 4. Contour variable is crossflow velocity $v_c = \sqrt{(v^2 + w^2)}/u_\infty$—eight levels, $0.05 < v_c < 0.5$. Both the vortex positions and the vortex strengths in the calculation show very good agreement to the measurement result.

The TAU result at $x/b = 0.5$ is used to initialize a subsequent two-dimensional EuLag calculation of the extended near field up to $x/b = 6$. The two-dimensional mesh has 501×401 points, the domain size is in horizontal direction $L_y = 2.15b$, and in vertical direction $L_z = 1.5b$. This leads to a resolution of the horizontal tail plane vortex with three points, ten points within the flap vortex, and seven points within the wing-tip vortex, which is a reasonable resolution for MILES as used by Dörnbrack et al.[14] in EuLag-validation calculations for vortex flow simulations.

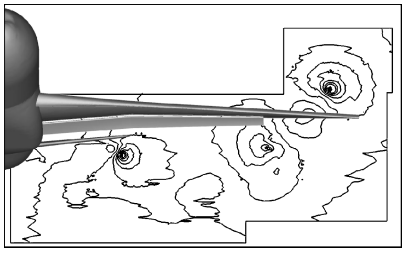

a) Experiment

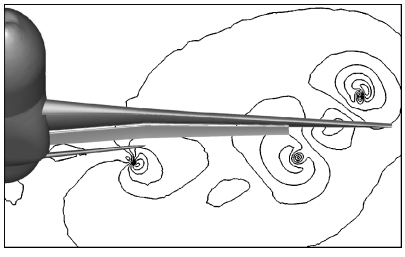

b) TAU result on seven times adapted mesh

Fig. 4 Near-field validation: comparison of crossflow velocity at $x/b = 0.5$; eight levels $0.05 < v_c < 0.5$.

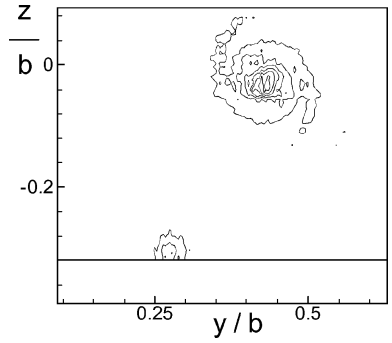

a) Experiment

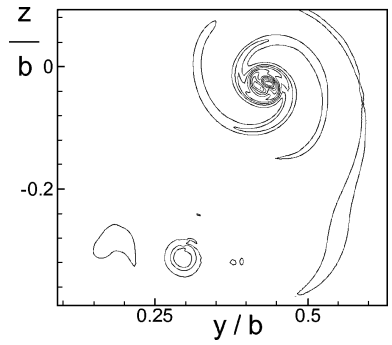

b) EuLag result, initialized with near-field TAU result

Fig. 5 Extended near-field validation: comparison of vorticity at $x/b = 6$; 15 levels $-5 \le (\omega_x b/2)/u_\infty \le 20$.

Figure 5 shows a comparison—experiment vs EuLag result—at $x/b = 6$. Contour variable is normalized axial vorticity—15 levels, $-5 \le (\omega_x b/2)/u_\infty \le 20$. As before, the vortex positions and the vortex strengths show very good agreement. This becomes even more clear in Fig. 6, which displays an enlarged view of the main vortex in Fig. 5. Both in the experiment (see Fig. 6a) and the calculation (see Fig. 6b), the wing and flap-tip vortices are not yet fully merged. The excellent agreement between these two vorticity peaks—remnants of the wing-tip vortex and the flap-tip vortex, respectively—are found in the center region in Figs. 6a and 6b.

Thus, the coupled three-dimensional Euler/two-dimensional-MILES simulation is capable both to capture qualitatively the main flow phenomena of the formation and development of the near- and extended near-field wake of an airliner in high-lift configuration and to simulate the flowfield variables quantitatively in good agreement to five-hole probe measurements up to $x/b = 6$.

Far-Field Validation

For the validation of the far-field calculation, a four-vortex system with the parameter settings: $\Gamma_2/\Gamma_1 = -0.35$, $b_2/b_1 = 0.5$, $r_1/b_1 = 5\%$, and $r_2/b_1 = 2.5\%$ is chosen. The same parameters have been used by Fabre (personal communication, 2003) in linear instability calculations, and the parameters of a towing experiment by Ortega[5] using particle-image-velocimetry (PIV) measurement technique are only slightly different. (In the Ortega case, the circulation ratio was $\Gamma_2/\Gamma_1 = -0.37$, and the radii were larger by a factor of 1.45.)

With periodic boundary conditions in axial direction, the longest wavelength to be resolved, namely, the wavelength of the Crow instability, dictates the domain length. Taking an analysis by Steijl,[19] the Crow wavelength corresponding to the radius of the outer vortex pair $r_1/b_1 = 0.05$ is $\lambda = 9.4285b$. The wavelength of the most amplified mode determined by Fabre (personal communication, 2003) is with $\lambda_{\text{short}} \approx 1/9\lambda_{\text{Crow}}$ approximately an integer factor. Thus, the simulation domain is chosen to comprise one Crow wavelength in axial direction resolved by 151 points. In the vertical direction 201

Table 1 Four-vortex test cases

Test case	b_2/b_1	Γ_2/Γ_1	$\Gamma_0=\Gamma_1+\Gamma_2$	r_1/b_1	r_2/b_1
1	0.35	−0.35	30.0 m²/s	5%	2.5%
2	0.5	−0.35	30.0 m²/s	5%	2.5%

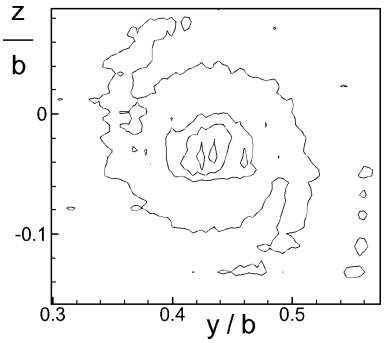

a) Experiment (enlarged)

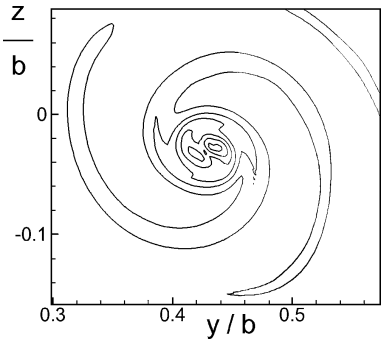

b) EuLag result, initialized with near-field TAU result (enlarged)

Fig. 6 Extended near-field validation: enlarged view of vorticity at $x/b=6$; seven levels $0.5 \le (\omega_x b/2)/u_\infty \le 20$.

points (domain height $2.5b$) and in the lateral direction 401 points (domain width $5b$) are distributed, slightly clustered in the center region. Again, the resolution is chosen to be similar to the validation simulations done by Dörnbrack et al.[14] The boundary conditions in axial direction are periodic; in horizontal and vertical direction free-slip walls are used. White noise similar to weak atmospheric turbulence with a rms value of $v_{\mathrm{RMS}}=0.005\times\max(v_\Theta)$ is superimposed.

Triggered by white noise, instabilities develop on the inner vortices in time showing different mean wavelengths on both sides. On the left side seven periods emerge ($\lambda_{\mathrm{left}}/b_1=L_x/7b_1=1.309$), whereas on the right side nine periods show up ($\lambda_{\mathrm{right}}/b_1=L_x/9b_1=1.047$). A similar behavior was observed by Ortega.[5] Furthermore, the value $\lambda_{\mathrm{left}}/b_1=1.309$ shows good agreement with the towing tank measurement ($\lambda_{\mathrm{exp.}}/b_1=1.3$). The value $\lambda_{\mathrm{right}}/b_1=1.047$ on the other hand is very close to the most amplified mode ($\lambda_{\mathrm{short}}/b_1=1.075$). The range of wavelengths λ and amplification rates σ on the left inner vortex is $0.94\le\lambda_{\mathrm{left}}/b_1\le1.51$ resp. $9.29\le\sigma_{\mathrm{left}}\le13.48$ and on the right inner vortex $0.7\le\lambda_{\mathrm{right}}/b_1\le1.26$ resp. $9.46\le\sigma_{\mathrm{right}}\le13.85$. Thus, as mandatory, the calculated amplification rates are lower than the maximum amplification rate of $\sigma_{\max}=14.48$ as determined by Fabre (personal communication, 2003).

After the linear phase of the instability, the inner vortices form Ω loops, which wrap around the main vortices. During this unstable merging process, two-dimensional kinetic energy $[E_{\mathrm{kin}}=\int\int 0.5(v^2+w^2)\,\mathrm{d}y\,\mathrm{d}z]$ is decreased. In Fig. 7 the temporal simulation result of the kinetic energy normalized with the initial kinetic energy is compared with towing tank PIV-measurements from Ortega.[5] On the abscissa the normalized time $t^*=[\Gamma_1/(2\pi b_1^2)]t$ is plotted. The PIV observation area in the experiment was small

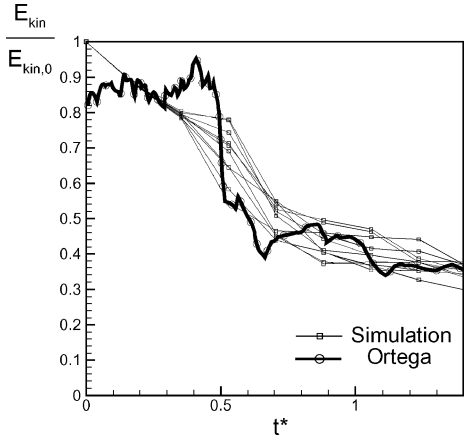

Fig. 7 Far-field validation: kinetic energy.

such that the initial value of $E_{\mathrm{kin}}/E_{\mathrm{kin},0}$ is unequal one. During the roll-up process of the wake, vorticity accumulated in the observation area, and the kinetic energy within the area increased up to the unstable merging process, which caused a sudden drop of E_{kin}. The normalized kinetic energy of the simulation is evaluated in 10 planes equidistantly distributed along the axial direction of the numerical domain. As can be seen in Fig. 7, the kinetic energy decreases monotonically, that is, the vortex radii increase, until $t^*=0.4$ as a result of numerical dissipation. But the energy drop during the unstable merging process is simulated in excellent agreement to the experiment. In both the experiment and the simulation the energy loss is $\Delta(E_{\mathrm{kin}}/E_{\mathrm{kin},0})\approx-60\%$. Within the proposed sequence of numerical simulations, the knowledge of the postmerging state is essential in order to identify an optimal four-vortex configuration. Temporal three-dimensional EuLag MILES meets this demand and is therefore used for the investigation of four-vortex systems in the proposed numerical strategy. However, an unresolved issue remains the low Reynolds number in the MILES simulations $Re_\Gamma\approx2.5\times10^3$. An extrapolation of the real size aircraft case from the simulation results should be done with care. The assessment of Reynolds-number effects on vortex wakes is a task in current European research activities.

Results

Four-Vortex Test Cases

In the present paper as a proof of concept only two different four-vortex configurations are investigated (details are listed in Table 1). If the aim is to identify a four-vortex system leading to a minimum rolling moment induced on following aircraft, a larger number of configurations would have to be simulated.

From previous investigations[7,8] it is known that a large negative circulation ratio is favorable. Thus, for both investigated four-vortex configurations a circulation ratio of $\Gamma_2/\Gamma_1=-0.35$ is chosen. Also identical in both test cases are the normalized vortex core radii $r_1/b_1=5\%$ and $r_2/b_1=2.5\%$, the main vortex spacing $b_1=2.8$ m, and the total circulation $\Gamma=30.0$ m²/s.

Different in both test cases is the vortex spacing ratio b_2/b_1—case 1, $b_2/b_1=0.35$; case 2, $b_2/b_1=0.5$. (Case 2 is identical to the far-field validation case.)

The two test cases are depicted in the Donaldson–Bilanin diagram in Fig. 8. Three areas can be distinguished in the diagram. The gray area comprises all parameter combinations that are divergent, that is, the inner vortex pair escapes vertically upward from the outer vortices. The white area is the periodic regime in which the inner vortices rotate continuously around the outer ones. It is claimed in Stuff[7] and Rossow[8] that a reduced hazard is obtained only if the circulation ratio of the counter-rotating vortex pair $|\Gamma_2/\Gamma_1|$ exceeds 20%. The analogical bold horizontal curve dividing the white area is taken from Stuff.[7] Furthermore, the diagram shows optimal growth rates calculated by Fabre.[3] The growth rate isolines at values $\Gamma_2/\Gamma_1<-0.2$ and $b_2/b_1>0.3$ are more or less parallel to the

ordinate; increased growth rates are only obtained with increased b_2/b_1. Thus, for the two chosen four-vortex configurations it can be expected that 1) the vortices show a periodic behavior; 2) the unstable merging leads to a significant rolling-moment reduction; and 3) the instability, and hence the merging process, occurs earlier in configuration 2.

First Step: Far-Field Four-Vortex Calculations

For the far-field four-vortex calculations, parameter settings identical to the settings in the far-field validation calculation are used for the flow solver and the mesh generator. The simulated time for both cases is $t^* = 1.76$ ($\widehat{=}$ 2.89 n miles for a real size Airbus A340 at 143 kn).

Figure 9 shows vorticity isosurfaces [displayed vorticity level is $|\omega| = 0.05 \times \max(|\omega_0|)$] of configuration 1 evolving in time. The upcoming short-wave instability can be seen at $t^* \geq 0.7$. Because weak atmospheric turbulence is used to trigger the instability, the development is not symmetric. The inner vortices form Ω loops, which wrap around the outer vortices. Vorticity stretching leads to a fast enlargement of the loops that collide in the symmetry plane, (Fig. 9d). After the dissipation of the scattered vorticity (see Fig. 9e and 9f), it becomes visible that the main vortices survive the chaotic merging process. The remaining counter-rotating vortex pair is clearly distorted but shows a coherent structure, no long wave instability, and is not likely to experience short-term disintegration.

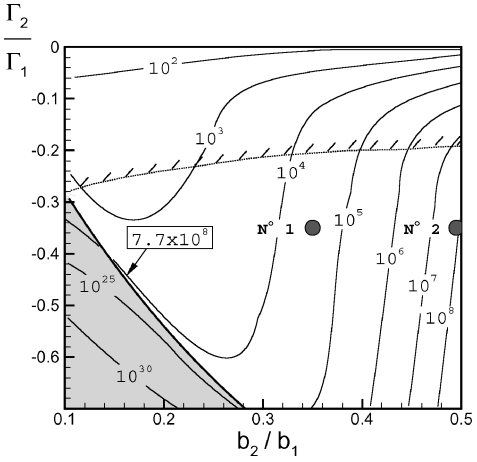

Fig. 8 Donaldson–Bilanin[20] diagram with results by Fabre et al.[4] and Stuff.[7]

In Fig. 10 the temporal development of configuration 2 is displayed. Because of the closer spacing of the inner and outer vortices, the rotation of the inner around the outer vortices is faster compared to configuration 1. As predicted in the theoretical investigation by Fabre,[3] the short-wave instability emerges earlier in configuration 2. This leads to smaller Ω loops and a huge amount of scattered vorticity. However, as observed for configuration 1, the main vortices survive the unstable merging process as deformed, but coherent vortex tubes (see Fig. 10f).

The isosurfaces of vorticity are a representation of the flow topology but do not provide an information if the hazard after merging can be considered benign. Therefore, a quantitative analysis of the temporal rolling-moment evolution of configuration 1 is given in Fig. 11 up to $t^* = 1.76$.

For vortex encounter here the considered scenario is a medium-class airplane (with half the span of the wake generator) flying into the vortex center of one of the two main vortices (which represent a heavy-class airplane wake). The rolling-moment coefficient c_R is calculated according to Condit and Tracy[21] by using

$$c_R = \frac{2\pi}{u_{\infty,f} S_f b_f} \int_{-b_f/2}^{b_f/2} y c_f(y) v_\Theta(y, 0)\, \mathrm{d}y \tag{1}$$

with $u_{\infty,f}$ being the speed of the following aircraft. The variable c_f denotes the chord, b_f the span, and S_f the wing area of the following aircraft.

To account for numerical dissipation effects, the calculated rolling moment is not given in absolute values, but analyzed relative to the simulation result for a two-vortex reference system, which was obtained on a mesh with the same resolution as used for the four-vortex configurations. Total circulation and vortex spacing b_1 of the reference two-vortex system and the four-vortex configuration are identical. The rolling moment c_R is on the one hand normalized with the value of the rolling moment $|c_{R,2V}|$ of the reference two-vortex system at a downstream distance equal to the separation distance (i.e., 5 n miles) and on the other hand with the ratio $c_L/c_{L,2V}$ of the lift coefficient c_L of the investigated four-vortex system and the lift coefficient $c_{L,2V}$ of the reference configuration. The rolling moment is evaluated in 10 planes equidistantly distributed along the axial direction of the numerical domain.

The magnitude of normalized maximum rolling-moment coefficient changes periodically, that is, it is maximum whenever the

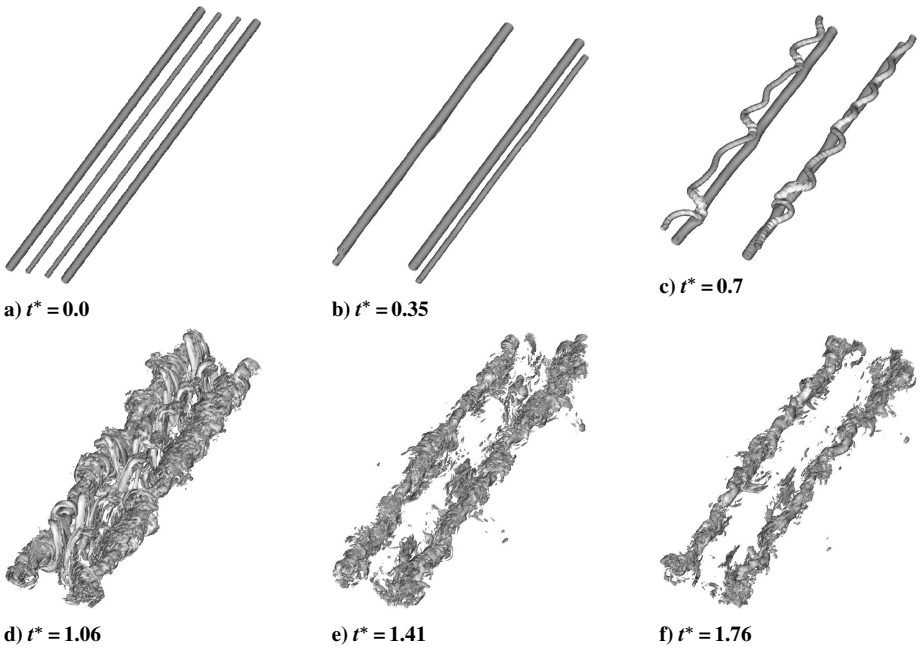

Fig. 9 Temporal development of isosurfaces of vorticity $|\omega| = 0.05 \times \max(|\omega_0|)$ of configuration 1.

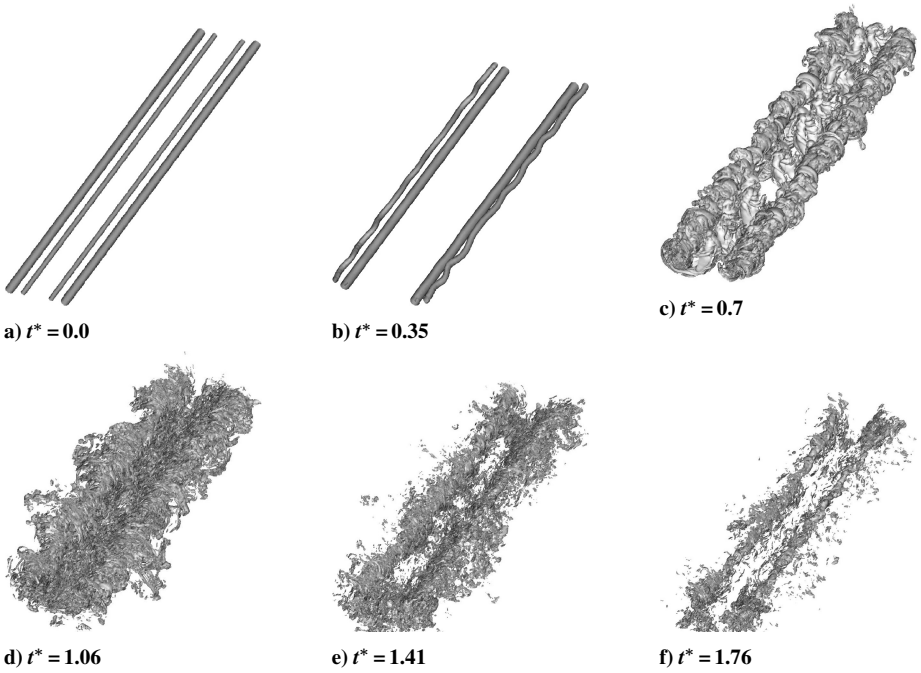

Fig. 10 Temporal development of isosurfaces of vorticity $|\omega| = 0.05 \times \max(|\omega_0|)$ of configuration 2.

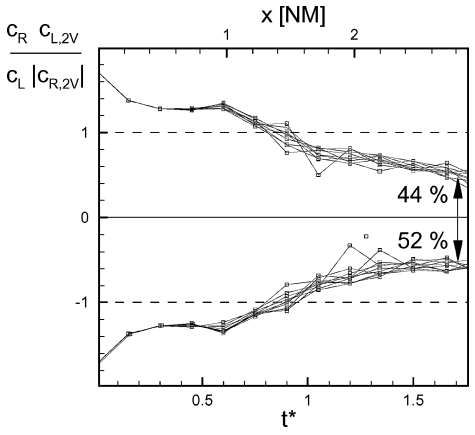

Fig. 11 Rolling-moment configuration 1.

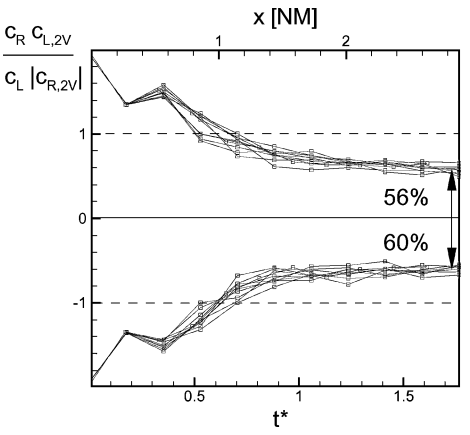

Fig. 12 Rolling-moment configuration 2.

orbiting inner vortices are in the horizontal plane with the outer vortices. In Fig. 11, the upper curves correspond to the maximum rolling moment found in the left main vortex in the 10 evaluated planes, whereas the lower curves correspond to the same but in the right main vortex. The lower abscissa shows the normalized time t^*; the upper one gives the traveled distance for a real size Airbus A340.

The initial rolling moment of the four-vortex configuration 1 is of course significantly higher than the rolling moment produced by the reference two-vortex system at 5 n miles, as can be seen in Fig. 11. While the inner vortices rotate around the outer vortices, the rolling moment changes, leading to local minimum once the inner vortices are found vertically below the outer vortices ($t^* = 0.3$) and to a local maximum at the time when the inner vortices lie outside of the main vortices in a horizontal plane with those ($t^* = 0.6$). With the start of the merging process of the counter-rotating inner and outer vortices, a significant decrease of rolling moment occurs at $t^* = 0.6$ and leads to a drop down to 44–52% of the maximum rolling moment of the reference two-vortex system until $t^* = 1.76$ (see Fig. 11). The steepest gradient of rolling-moment decrease is found in the start of the merging phase. Once the inner vortices are disintegrated, the vorticity debris dissipates, and the gradient of the temporal development of the rolling moment tends to zero (see Fig. 11).

The temporal development of the rolling-moment coefficient of configuration 2 is shown in Fig. 12. Here, the sudden decrease of rolling moment occurs already at $t^* = 0.4$ because of the early onset of instability, but the overall gain in rolling-moment reduction is less than for case 1. Until $t^* = 1.76$ the rolling moment decreases to 56–60% of the maximum rolling moment of the reference two-vortex system.

Thus, the present investigation shows that a higher amplification rate leading to an early merging of counter-rotating vortices not necessarily results in lower rolling moments after merging. In contrast the configuration that exhibits later merging leads to gradually lower levels of rolling moment. This result is in agreement with experimental investigations by Haverkamp et al.[22] However, recent towing tank measurements by Durston et al.[23] show the opposite behavior. Higher spacing ratios lead in their investigations to lower rolling moments. But the general result that four-vortex systems of comparable circulation ratios produce a rolling-moment drop down to roughly 50% of the maximum rolling moment of a reference two-vortex system is confirmed by Durston et al.[23]

Because circulation and spacing ratio, Reynolds number, and turbulence level all differ somewhat in the experimentally and numerically investigated configurations, no final answer can be given here.

The interaction is highly nonlinear such that the choice of the initial condition is crucial.

Second Step: Layout of Corresponding Configurations

Following the reasoning of the sequence of numerical simulations, only the layout for the determined optimal four-vortex system would be necessary. In contrast, in the present paper the layout of a corresponding high-lift configuration is done for both investigated four-vortex configurations in order to prove the feasibility of such layout.

The high-lift configuration to be modified is the DLR-F11 model (see Fig. 2). The lift coefficient is kept constant for all modified configurations with $c_L = 1.76$.

The modification in the proposed sequence is done by hand, which implies that the realization of the desired four-vortex system remains an engineering problem. Besides the existing vortices from the wing, flap, and horizontal-tail side edges, possibly additional artificial vortices have to be generated by means of, for example, fins or wish bones, if handling quality, maximum lift coefficient, and center of gravity position are to be maintained as required for certification. In the present paper the aim is to prove the general feasibility of a target-oriented modification that results in a predefined four-vortex system. Therefore, as a simplification, in the presented layout process the configuration modifications are restricted to changes of the horizontal-tail-plane setting and to individual changes of flap segment deflection angles. Hence, handling quality, maximum lift coefficient, and c.g. position are at this stage not accounted for.

Layout of Configuration 1

The parameters of configuration 1 are $\Gamma_2/\Gamma_1 = -0.35$ and $b_2/b_1 = 0.35$. The ratio of the horizontal-tail-plane span to the wing span of the DLR-F11 amounts to $b_{\mathrm{HTP}}/b = 0.375$. Because not only the roll-up process is dependent on the aspect ratio ($\Lambda_{\mathrm{wing}} > \Lambda_{\mathrm{HTP}} \Rightarrow b_{\mathrm{HTP}}/b_{\mathrm{HTP},0} < b/b_0$) but also the flap creates a strong corotating vortex at the outer flap side edge, the distance ratio of the rolled-up vortices $b_{\mathrm{HTP},0}/b_0$ will evolve towards the desired value of 0.35. With known airfoil data of the horizontal tail plane and estimations of the downwash from Torenbeek,[4] the required horizontal-tail-plane deflection can be calculated. This value amounts to $\delta_{\mathrm{HTP}} = -12.3$ deg.

Layout of Configuration 2

The parameters of configuration 2 are $\Gamma_2/\Gamma_1 = -0.35$ and $b_2/b_1 = 0.5$. Because vorticity sheets strictly roll up from the sides towards the sheet centerline, the opportunity arises to employ the vortex sheet and inboard vortex of the outboard flap segment. The maximum effect is achieved if the inboard flap is completely retracted. The ratio of the inboard flap side-edge position and the wing span is $b_{\mathrm{iflap}}/b = 0.365$. Assuming elliptic loading for the outboard flap and the wing, the ratio of the inboard flap side-edge position and the estimated centroid position of the outer flap vortex and wing-tip vortex increases to $[2 - (\pi/4)]b_{\mathrm{iflap}}/[(\pi/4)b] = 0.53$. The circulation ratio can to a certain extent be varied with the flap deflection angle. Here, the flap is set to $\delta_{\mathrm{flap}} = 32$ deg.

Third Step: Wake-Vortex Calculations of Modified Aircraft Configurations

To verify the existence of a four-vortex wake of the modified airliner configurations and the similarity to the aforedetermined four-vortex systems, the near and extended near fields of the two modified aircraft configurations are calculated. For the calculations parameter settings identical to the settings in the near- and extended near-field validation calculations are used for the flow solvers, the adaptation module, and mesh generators.

Near-Field Calculations of Configurations 1 and 2

Figure 13 shows vorticity and total pressure loss contour plots of configuration 1 at $x/b = 0.5$. For obtaining a lift coefficient of $c_L = 1.76$, an angle of attack of $\alpha = 10.9$ deg is needed. The corotating flap-tip and wing-tip vortices are rotated around each other by

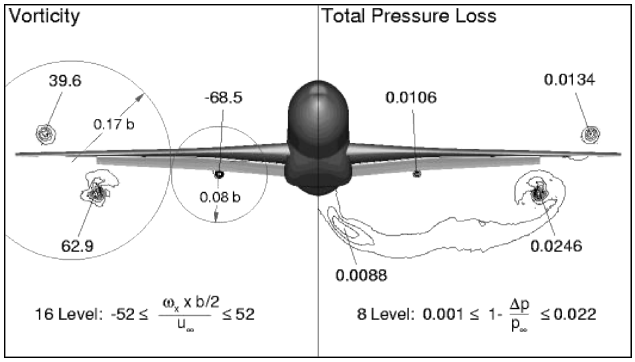

Fig. 13 Layout of configuration 1 at $x/b = 0.5$.

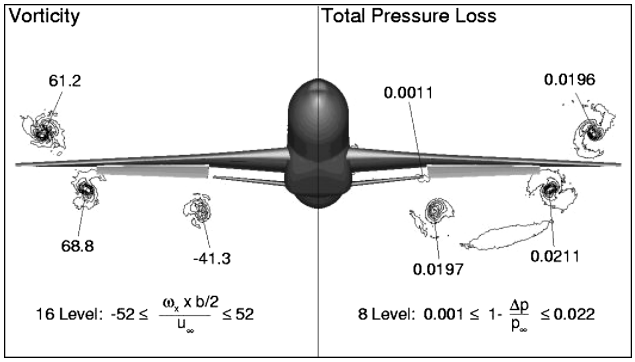

Fig. 14 Layout of configuration 2 at $x/b = 0.5$.

$\frac{1}{8}$ revolution. The two vortices will eventually merge on both sides of the symmetry plane. The counter-rotating inner vortex pair is represented by the horizontal-tail vortices. Because of the perspective view, the horizontal-tail plane is hidden, but below the flaps the horizontal-tail-plane vortices are visible.

The integration limits for the determination of the centroid position of flap- and wing-tip vortex, horizontal-tail-plane vortex, and respective circulations are depicted on the left side of Fig. 13. In most cases such simple circular limits do not contain exactly the vorticity, which will roll up into the four-vortex-wake configuration, rather this evaluation at $x/b = 0.5$ gives an approximate picture. Thus, the subsequent two-dimensional MILES calculation of the roll-up process is mandatory to obtain an exact information about circulation and spacing ratio of the developping four-vortex system.

In Fig. 14 vorticity and total pressure loss contour plots of configuration 2 at $x/b = 0.5$ are displayed. To maintain the lift coefficient of $c_L = 1.76$, the angle of attack is increased to $\alpha = 15.1$ deg. As in configuration 1, the corotating flap-tip and wing-tip vortices are rotated around each other by $\frac{1}{8}$ revolution. The counter-rotating inner vortex pair in configuration 2 is represented by the vortices from the inner side edges of the outer flaps.

Extended Near-Field Calculations of Configurations 1 and 2

The complete wake development of configuration 1 including the subsequent two-dimensional simulation result is shown as vorticity isosurfaces in Fig. 15. It can be seen that the flap- and wing-tip vortices merge at $x/b \approx 6$; downstream a four-vortex system evolves.

The wake-vortex evolution of configuration 2 up to $x/b = 10$ is shown as vorticity isosurfaces in Fig. 16. The flap- and wing-tip vortices merge at $x/b \approx 6.5$, such that as in configuration 1 downstream the desired four-vortex system evolves.

Quantitative Analysis of Configurations 1 and 2

The quantitative analysis of the circulation and spacing ratio at $x/b = 0.5$ (dark-grey square symbol) and $x/b = 10$ (light-grey square symbol) is displayed in Fig. 17. For configuration 1 it can be seen that the inner vortex pair, that is, the horizontal-tail-plane vortices, are too weak. The target four-vortex parameters of

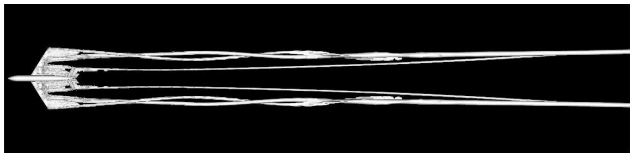

Fig. 15 Vorticity isosurface configuration 1 ($0 \le x/b \le 10$).

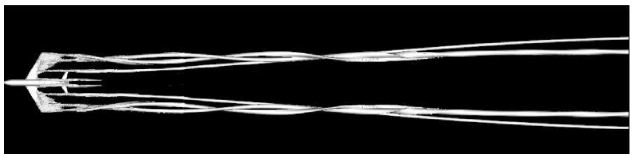

Fig. 16 Vorticity isosurface configuration 2 ($0 \le x/b \le 10$).

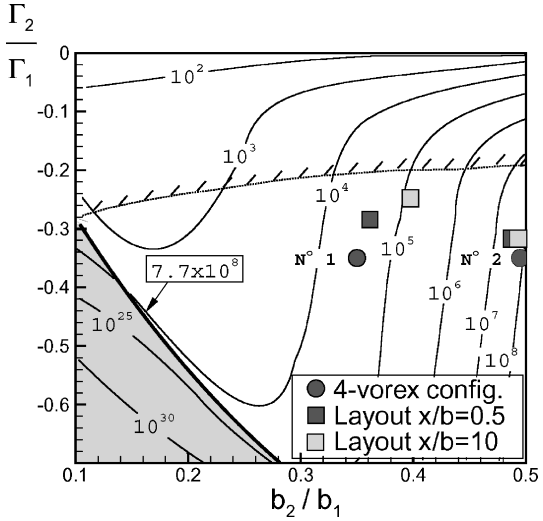

Fig. 17 Parameters of layout of configurations 1 and 2.

configuration 1 are $\Gamma_2/\Gamma_1 = -0.35$ and $b_2/b_1 = 0.35$. The approximate evaluation at $x/b = 0.5$ of the layout of the modified DLR-F11 model gives $\Gamma_2/\Gamma_1 = -0.29$ and $b_2/b_1 = 0.36$. But the more exact analysis at $x/b = 10$ shows with $\Gamma_2/\Gamma_1 = -0.25$ and $b_2/b_1 = 0.4$ that the target parameters are not well reached. Here, only one iteration is done. To obtain a better agreement for configuration 1, a second iteration step with increased horizontal-tail-plane deflection would be needed.

The quantitative analysis for configuration 2 shows that the agreement between four-vortex configuration and actual wake vortex behind the modified DLR-F11 is very good, both for the downstream plane at $x/b = 0.5$ with $\Gamma_2/\Gamma_1 = -0.31$ and $b_2/b_1 = 0.48$ as well as for the downstream plane at $x/b = 10$ with $\Gamma_2/\Gamma_1 = -0.31$ and $b_2/b_1 = 0.50$. Thus, for configuration 2 the chosen integration limits at $x/b = 0.5$ are rather exact, and a single iteration step is sufficient to produce the desired four-vortex topology in the wake of the modified DLR-F11 model.

Conclusions

A sequence of numerical simulations has been proposed and demonstrated to be capable to identify generic four-vortex configurations, consisting of two counter-rotating vortex pairs, with low induced rolling moments after the unstable merging of inner and outer vortices. Furthermore, the sequence allows the realization of four-vortex wakes behind modified high-lift configurations similar to afore-determined promising generic four-vortex configurations.

Some conclusions can be drawn from the investigation:

1) Four-vortex wakes have been shown to have the potential to alleviate the wake-vortex hazard. This conclusion holds at least for low-Reynolds-number flows. However, Rossow[8] found indications in free-flight tests with a Boeing 747 that four-vortex wakes are effective. Thus, aircraft configurations producing four-vortex wakes should be further investigated. Currently corresponding free-flight tests are envisaged in the European research project AWIATOR.

2) For both investigated generic four-vortex configurations with a circulation ratio of $\Gamma_2/\Gamma_1 = -0.35$, a significant rolling-moment reduction has been observed after the unstable merging process. This supports the prediction of Rossow[8] and Stuff[7] that the circulation ratio of a four-vortex system has to exceed 20% to be effective.

3) The merging point in time seems to be an essential parameter. An early merging, as found in configuration 2 (close spacing of inner and outer vortices), produced a rolling-moment reduction down to 56–60% of the maximum rolling moment of the reference two-vortex system. The rolling-moment reduction during late merging (configuration 1) was more favorable with 44–52%.

4) The investigated instabilities are triggered by white noise representing weak atmospheric turbulence. Thus, the mechanism relies on the meteorological conditions. However, no active system is needed for an onset of instability.

5) Because triggered by weak atmospheric turbulence, always the most amplified instability mode will dominate the vortex development. This is in general not the Crow instability, which is, according to present knowledge, the most efficient source of wake-vortex alleviation. In the investigated cases the Crow instability did not become visible, which supports the conclusion by Fabre and Jacquin[3] that the Crow instability has to be actively triggered to be effective within the ATC separation distance.

6) For both generic four-vortex configurations the layout of a corresponding high-lift configuration was successful. However, in the present investigation handling quality, maximum lift coefficient, and c.g. position were not accounted for, and the considered aircraft geometry, namely, the DLR-F11, is not equipped with engine nacelles, flap track fairings, and other vorticity sources of realistic configurations.

Acknowledgments

The present work has been funded by the DLR research project Wirbelschleppe. Some results have been validated with data obtained within the framework of the C-Wake program, funded by the European Commission (Contract G4RD-CT-1999-000141). The author is grateful to P. Smolarkiewicz and to all involved partners.

References

[1]Crow, S. C., and Bate, E. R., "Lifespan of Trailing Vortices in a Turbulent Atmosphere," *Journal of Aircraft*, Vol. 13, No. 7, 1976, pp. 476–482.

[2]Crouch, J. D., and Spalart, P., "Active System for Early Destruction of Trailing Vortices," U.S. Patent PTC/US98/11569, 1998.

[3]Fabre, D., and Jacquin, L., "Stability of a Four-Vortex Aircraft Wake Model," *Physics of Fluids*, Vol. 12, No. 10, 2000, pp. 2438–2443.

[4]Fabre, D., Jacquin, L., and Loof, A., "Optimal Perturbations in a Four-Vortex Aircraft Wake in Counter-Rotating Configuration," *Journal of Fluid Mechanics*, Vol. 451, Jan. 2002, pp. 319–328.

[5]Ortega, J. M., "Stability Characteristics of Counter-Rotating Vortex-Pairs in the Wakes of Triangular-Flapped Airfoils," Ph.D. Dissertation, Dept. of the Chemical Engineering, Univ. of California, Berkeley, April 2001.

[6]Coton, P., "Characterization and Modification of Wakes from Lift: Vehicles in Fluids," AGARD CP-584, May 1996, pp. 29-1–29-12.

[7]Stuff, R., "Relationship Between Near- and Farfield of Vortex Wakes from Aircraft with High-Aspect Ratio Wings," *Notes on Numerical Fluid Mechanics*, Vol. 77, Nov. 2002, pp. 58–65.

[8]Rossow, V. J., "Lift-Generated Vortex Wakes of Subsonic Transport Aircraft," *Progress in Aerospace Sciences*, Vol. 35, No. 6, 1999, pp. 507–660.

[9]Torenbeek, E., *Synthesis of Subsonic Airplane Design*, Kluwer Academic, Norwell, MA, 1982.

[10]Domradzki, J. A., Xiao, Z., and Smolarkiewicz, P. K., "Effective Eddy Viscosities in Implicit Large Eddy Simulations of Turbulent Flows," *Physics of Fluids*, Vol. 15, No. 12, 2003, pp. 3890–3893.

[11]Gerhold, T., Friedrich, O., and Evans, J., "Calculations of Complex Three-Dimensional Configurations Employing the DLR-τ-Code," AIAA Paper 97-0167, Jan. 1997.

[12]Smolarkiewicz, P. K., and Margolin, L. G., "MPDATA: A Finite-Difference Solver for Geophysical Flows," *Journal of Computational Physics*, No. 140, No. 2, March 1998, pp. 459–479.

[13]Boris, J. P., Grinstein, F. F., Oran, E. S., and Kolbe, R. L., "New Insights into Large Eddy Simulation," *Fluid Dynamic Research*, Vol. 10, 1992, pp. 199–228.

[14]Dörnbrack, A., Stumpf, E., Prusa, J. M., and Smolarkiewicz, P. K., "Two and Three Dimensional Vortex Decay Simulated by Nonoscillatory Forward-in-Time Schemes," *Proceedings of the EuroMech Colloquium*, Dynamics of Trailing Vortices, No. 433, March 2002.

[15]Stumpf, E., "Numerical Investigation of the Effect of the High-Lift Configuration of a Transport Aircraft on its Vortex Wake," *Notes on Numerical Fluid Mechanics*, Vol. 77, Nov. 2002, pp. 50–57.

[16]de Bruin, A. C., Hegen, S. H., Rohne, P. B., and Spalart, P. R., "Flow Field Survey in Trailing Vortex-System Begind a Civil Aircraft Model at High Lift," AGARD CP-584, May 1996, pp. 25-1–25-12.

[17]Coustols, E., Stumpf, E., Jacquin, L., Moens, F., Vollmers, H., and Gerz, T., "Minimised Wake: a Collaborative Research Programme on Aircraft Wake Vortices," AIAA Paper 2003-938, Jan. 2003.

[18]Stumpf, E., Hepperle, M., Darracq, D., Meese, E. A., Elphick, G., and Galpin, S., "Benchmark Test for Euler Calculations of a High Lift Configuration Vortex Wake," AIAA Paper 2002-0554, Jan. 2002.

[19]Steijl, R., "Computational Study of Vortex Pair Dynamics," Ph.D. Dissertation, Dept. of Mechanical Engineering, Univ. of Twente, Dec. 2001.

[20]Donaldson, D., duPont, C., and Bilanin, A., "Vortex Wakes of Conventional Aircraft," AGARDOgraph No. 204, Aeronautica Research Association of Princeton, Princeton, NJ, May 1975.

[21]Condit, P. M., and Tracy, P. W., "Results of the Boeing Company Wake Turbulence Test Program," *Aircraft Wake Turbulence and Its Detection*, Plenum, New York, 1971, pp. 473–508.

[22]Haverkamp, S., Jacob, D., and Neuwerth, G., "Studies on the Influence of Outboard Flaps on the Vortex Wake of a Rectangular Wing," *Aerospace Science and Technology*, Vol. 7, No. 5, 2003, pp. 331–339.

[23]Durtson, D., Walker, S., Driver, D., Smith, S., and Savas, O., "Wake Vortex Alleviation Flow Field Studies," AIAA Paper 2004-1073, Jan. 2004.